

UC Berkeley

UC Berkeley Previously Published Works

Title

Understanding the Solvation Structure of Li-Ion Battery Electrolytes Using DFT-Based Computation and ^1H NMR Spectroscopy

Permalink

<https://escholarship.org/uc/item/4rc4z280>

Journal

The Journal of Physical Chemistry B, 126(47)

ISSN

1520-6106

Authors

Im, Julia

Halat, David M

Fang, Chao

et al.

Publication Date

2022-12-01

DOI

10.1021/acs.jpcc.2c06415

Peer reviewed

Understanding the Solvation Structure of Li-ion Battery Electrolytes Using DFT-based Computation and ¹H NMR Spectroscopy

Julia Im,¹ David M. Halat,^{1,2} Chao Fang,^{1,2} Darby T. Hickson,^{1,2} Rui Wang,^{1,2} Nitash P. Balsara,^{1,2} Jeffrey A. Reimer^{1,2,*}

¹*Department of Chemical and Biomolecular Engineering, University of California, Berkeley, Berkeley, California 94720, United States*

²*Materials Sciences Division and Joint Center for Energy Storage Research (JCESR), Lawrence Berkeley National Laboratory, Berkeley, California 94720, United States*

* reimer@berkeley.edu

Abstract

Molecular dynamics (MD) simulations, density functional theory (DFT) calculations, and ¹H NMR spectroscopy were performed to gain a complementary understanding of the concentrated Li-ion electrolyte system, lithium bis(trifluoromethanesulfonyl)imide (Li[TFSI]) dissolved in tetraglyme. The computational methods provided the concentration dependence of differing solvation structure motifs by reference to changes in the corresponding NMR spectra. By combining both the computational and experimental methodologies we show that the various solvation structures, dominated by the coordination between the tetraglyme (G4) solvent and lithium cation, directly influence the chemical shift separation of resonances in the ¹H NMR spectra of the solvent. Thus, the ¹H NMR spectra can be used to predict the fraction of tetraglyme involved in the solvation process, with quantitative agreement with solvation fraction predictions from MD simulation snapshots. Overall, our results demonstrate the reliability of a hybrid computational and experimental methodology to understand the solvation structure and hence transport mechanism of LiTFSI-G4 electrolytes in the low concentration region.

Introduction

Ionic liquids (ILs) are low melting-point solvents useful for a wide range of applications, including electrolytes in batteries, supercapacitors, and dye-sensitized solar cells.¹⁻⁷ For example, solvate ionic liquids (SILs) represent one sub-class of ionic liquids that comprise concentrated solutions of salt in a molecular solvent with high donor number. SILs are characterized by strong coordination of solvent to the dissolved ions, typically cations, to form stable, long-lived complexes. Such electrolytes are an example of IL utility for Li-ion battery applications because they contain only the working cation (Li⁺), as opposed to mixtures of Li-containing salts and traditional ionic liquids, that contain two types of cations and as a consequence may possess low Li⁺ transference.⁸ Glymes (i.e., methoxy-terminated oligoethers, CH₃O(CH₂CH₂O)_nCH₃) are promising solvents commonly used as components of Li-ion battery electrolyte systems. Glyme-based systems, such as lithium bis(trifluoromethanesulfonyl)imide (Li[TFSI]) salt dissolved in tetraglyme (G4), have been extensively developed and explored.^{1,9-12} Recent work has shown this class of electrolytes undergoes greatly reduced decomposition in full battery cells compared to standard carbonate-based systems, enabling use of more experimental electrode materials and extending cycle life.¹³

Tetraglyme, which constitutes a typical molecular solvent of the SIL system, has also proven its potential in Li-ion batteries and supercapacitors; it is a small-molecule analog of the quintessential poly(ethylene oxide) [PEO] material used as a solid-state polymer electrolyte and its study can thus also provide insight into the ion transport mechanisms in polymer electrolytes.¹⁴ For example, typical characteristics of tetraglyme-based electrolytes as used in battery applications are high solubility of alkaline salts as well as high ionic conductivity.¹⁴

We surmise that developing more effective and more applicable battery electrolyte systems will rely on quantitative understanding of the mechanisms of ion solvation as revealed by local solvation structure,¹⁴ allowing for further, fine-tuned control of the electrolyte properties.¹⁵ Various computational efforts have been undertaken to analyze the structure–property relationships in Li-ion battery electrolyte systems, using methods such as molecular dynamics (MD) simulations and density functional theory (DFT) calculations.^{1,15} It has been mentioned previously that solely relying on computational methods to predict and analyze electrolytes, without recourse to experimental techniques such as spectroscopy, may lead to inaccurate conclusions.¹⁵

With the intention of providing further understanding of the LiTFSI-G4 electrolyte system, as well as to further complement the use of simulations as a computational tool for this system, we carried out a series of MD simulations to understand the solvation structure and dynamics as a function of Li-ion salt concentration.¹⁶ Results from MD simulations were evaluated with DFT modelling to predict ¹H NMR results, which were subsequently compared with experimental ¹H NMR shifts, thereby supporting the specific solvation structures. Our results reveal the local solvation structure of glyme-based electrolyte systems in the low concentration regime (i.e., below 2.5 *m* or 2 M) by combining DFT calculation, MD simulation, and NMR spectroscopy. Furthermore, our results provide insight into the specific nature and dynamics of the interactions between the tetraglyme molecular solvent and the lithium cation.

Methodology

Density functional theory calculations — DFT-based geometry optimization and NMR chemical shift prediction was conducted with the quantum chemistry Gaussian software.¹⁷ The basic molecular geometries were constructed using the auto-optimize tool of the Avogadro software¹⁸ using the Merck Molecular Force Field (MMFF94¹⁹) and Universal Force Field (UFF²⁰). MMFF94 was the default force field used for optimizing tetraglyme and UFF was used for structures containing Li⁺ and TFSI⁻ ions. The geometries were then optimized using the standard Gaussian method with the Becke, 3-parameter, Lee-Yang-Parr (B3LYP) functional,^{21,22} and using 6-31G(d) as the basis set. **Following the calculations, frequency calculations were performed to confirm that the geometry-optimized conformation was at its energy minimum.** NMR calculations were performed in Gaussian with the same level of theory and the same basis set as the geometry optimization calculations. **Multiple functional and basis sets were compared, and the B3LYP/6-31G(d) combination was found to be sufficiently accurate (closely resembles the experimental results) with much greater time efficiency given the large number of structures considered.**

Sample preparation and ¹H NMR spectroscopy — LiTFSI-G4 mixtures were prepared in a concentration range of 0.18 to 2.5 mol/kg of solvent. Herein the concentration of the samples is

defined by $r = [\text{Li}^+]/[\text{O}]$, the ratio between the concentration of lithium cations and that of the oxygen atoms in tetraglyme, for consistency with previous work.¹⁶ ^1H NMR spectra were acquired on the samples to identify the relative shifts of the resonances corresponding to protons within CH_2 and CH_3 groups of the tetraglyme solvent; additionally, ^1H T_1 (spin–spin relaxation) measurements were performed using a standard inversion recovery sequence. ^1H NMR experiments were performed at a field strength of 16.4 T using a 700 MHz Bruker Avance I spectrometer, equipped with either a Bruker 5 mm double-resonance broadband observe (BBO) probe or a Bruker 5 mm triple-resonance inverse (TXI) probe, with variable-temperature control. Measurements were performed using a Larmor frequency of 700.1 MHz. The sample temperature was fixed at 30 °C.

Molecular dynamics simulations — MD simulations were conducted on the LiTFSI-G4 electrolyte system. The selection of force fields for the LiTFSI salt and tetraglyme solvent as well as the simulation methods is similar to these reported previously.¹⁶ In brief, the Transferable Potentials for Phase Equilibria with United Atom description (TraPPE-UA) force field is used for tetraglyme molecule.^{23,24} The compatible all-atom force field is used for LiTFSI salt.²⁵ MD simulations are performed in the NPT ensemble (303K, 1bar) using the Gromacs code.²⁶ The temperature is maintained using the velocity-rescale thermostat,²⁷ while the pressure is kept using the Berendsen barostat.²⁸ The bonds of tetraglyme molecules are constrained using the LINCS algorithm.²⁹ The non-electrostatic and electrostatic interactions are computed using the cutoff method (cutoff length: 1.2 nm) and the particle mesh Ewald (PME) method³⁰, respectively. **The box size ranges from 3.3 nm to 3.6 nm. The number of tetraglyme molecules are set to 100, and the number of Li^+ and TFSI ions vary based on our experimental salt concentration.**

The time autocorrelation functions are defined to evaluate the time scales of the dominant solvation motifs.³¹ For a specific motif (see below), it is defined as $C_{\text{motif}}(t) = \langle P_m(t)P_m(0) \rangle / \langle P_m(0)P_m(0) \rangle$, where $\langle \dots \rangle$ denotes the ensemble average that is collected from all available motifs of the same type. $P_m(t)$ is a binary function, which is equal to 1 when an individual motif is always made of the same ions and G4 molecules over time t and is equal to 0 otherwise.

Results and Discussion

The local solvation structure and dynamics of an electrolyte system, which ultimately dictate functional properties such as conductivity and transference, are defined by the interactions between the salt and the molecular solvent. Specifically, the LiTFSI-G4 electrolyte system is characterized by the solvation interactions of the lithium cation, the TFSI⁻ anion (depicted in Figure 1a), and tetraglyme as the molecular solvent (depicted in Figure 1b). From the NMR perspective, the tetraglyme molecule possesses four distinct proton environments that translate to four different proton chemical shift values in the ^1H NMR spectra of tetraglyme. Consequently,

perturbations of these resonances in the presence of LiTFSI can potentially be used to understand solvation motifs and the corresponding dynamics of the electrolyte system as a function of salt concentration.

Figure 1b depicts the ^1H NMR spectrum of neat tetraglyme, along with the tetraglyme chemical structure, showing the correspondence between each NMR resonance and the proton environments. For the purposes of this study, the four different proton environments are arbitrarily labeled A–D, from highest to lowest observed chemical shift in the neat solvent; “D” corresponds to the end methyl (CH_3) groups, and “A” represents the middle methylene (CH_2) groups (Figure 1b), while “B” and “C” are the CH_2 groups nearer to the terminating methyl groups. Here, the proton chemical shift values have been taken from the AIST (Advanced Industrial Science and Technology) NMR spectral database, SDBS; the spectrum has been simulated from the reported shifts, and the effects of J -coupling are ignored.³² The chemical shift relies upon the relative amount of shielding and deshielding of the magnetic field experienced by the proton caused by local electronic interactions.³³ The “A” middle CH_2 groups are assigned to the highest chemical shift due to proximity to nearby electronegative oxygen atoms, unlike the other groups that lie closer to the end methyl groups without oxygen atoms. In this work, the significance of the NMR spectra relies on an understanding of how cation solvation-induced changes of the local proton environment affect the position of the NMR resonances. Specifically, this study focuses on the relative ^1H chemical shift values, quantified as the shift difference between observed peaks, rather than changes in the absolute values of the chemical shifts, which may be subject to bulk effects such as magnetic susceptibility that do not report on the local solvation structure.

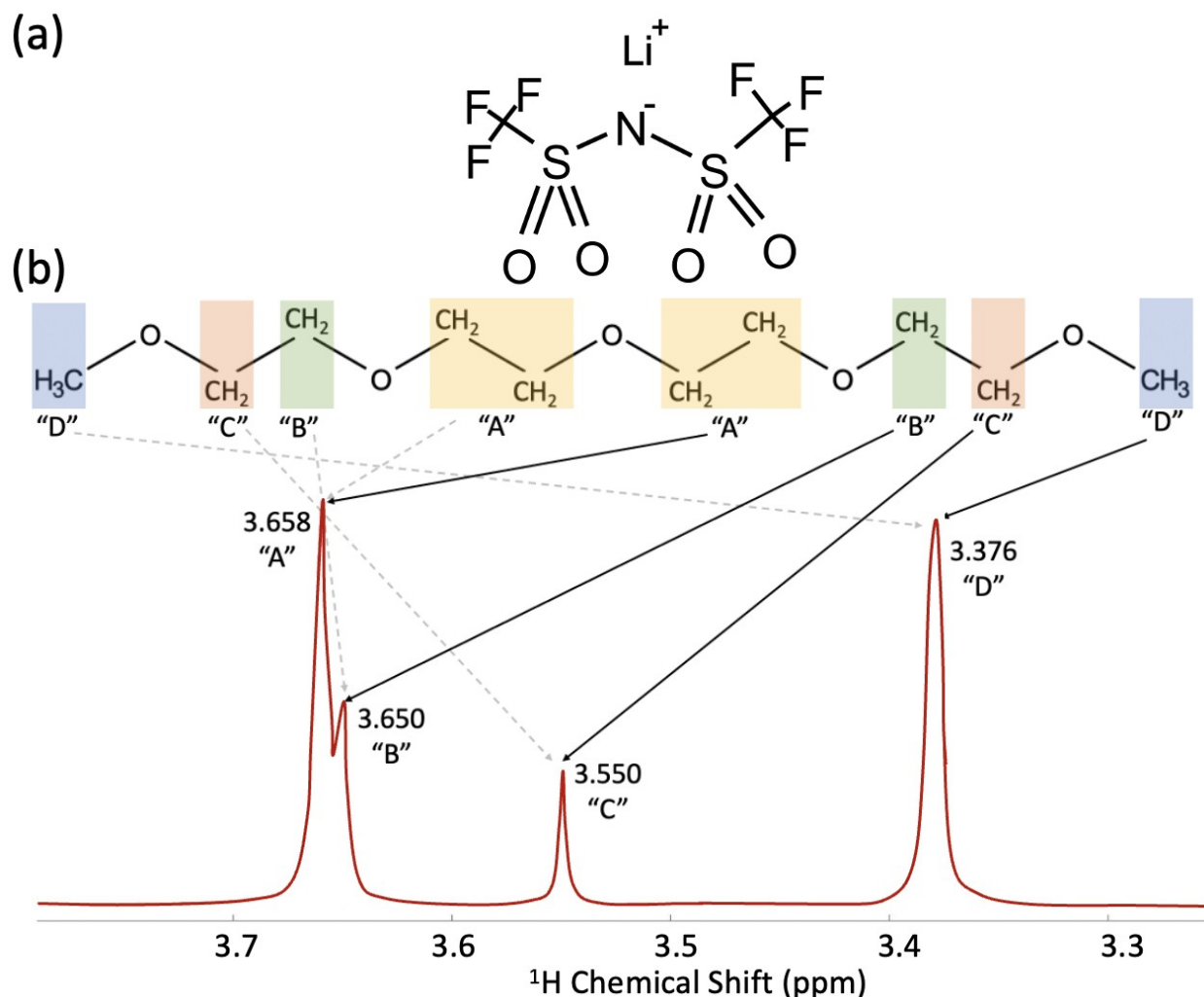


Figure 1. The overall chemical structure of the LiTFSI-G4 electrolyte system: (a) the chemical structure of LiTFSI salt, and (b) the chemical structure of tetraglyme with its corresponding simulated ^1H NMR spectrum. Color coding differentiates the different proton environments (A-D) ordered by decreasing ^1H shift, with the arrows indicating the peaks of the corresponding proton environment in tetraglyme. Note that the depicted spectrum has been simulated with arbitrary peak intensity, using the previously reported ^1H shifts of neat tetraglyme, and does not account for scalar (J) coupling effects.

In order to assess the sensitivity of the NMR spectra to changes in local solvation structure, we first investigated the different solvation structures of the LiTFSI-G4 electrolyte system. Solvation motifs were extracted from MD simulation¹⁶ and then further geometry-optimized using hybrid functional DFT calculations. In this way, we could understand the evolution of the distinct types of solvation motifs as a function of salt concentration ($r = [\text{Li}^+]/[\text{O}]$, the ratio between the concentration of lithium cations and that of the oxygen atoms in tetraglyme). Figure 2 presents the three dominant dynamically heterogeneous³⁴ motifs evident in the electrolyte system, as determined by analysis of the MD simulations.¹⁶ As described previously, these motifs have been extracted by considering the local environments of lithium cations in static snapshots of the MD simulations. These motifs correspond to (1) free solvent

molecules (Figure 2a), (2) “two-chain” motifs with two solvent molecules and one cation (Figure 2b, c), and (3) “one-chain” motifs with two solvent molecule, two cation and one anion (Figure 2d). The free solvent motif represents the structure of the tetraglyme molecule when the oxygens of the tetraglyme molecules are not directly coordinated to lithium cations. With increasing salt concentration, the dominant solvation structure shifts to two-chain motifs representing a 2:1 ratio between tetraglyme molecules and lithium cations, with two tetraglyme molecules providing coordinating oxygen sites for one lithium cation. The one-chain motifs become the predominant solvation structure at higher concentrations, which results from the increase in the amount of lithium cations available in comparison to the amount of tetraglyme. These motifs comprise a coordination ratio of 1:1, with one tetraglyme molecule surrounding one lithium cation, and the TFSI⁻ anions providing the remaining oxygen sites for coordination (Figure 2d).

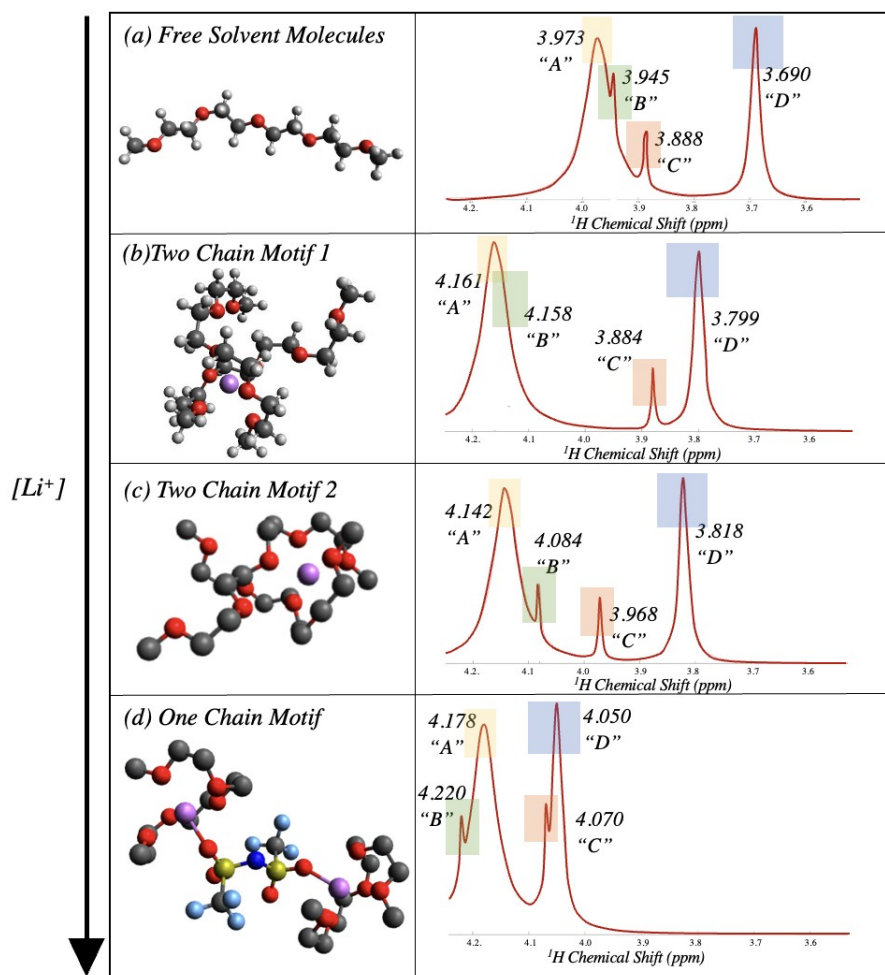


Figure 2. Solvation motifs of the LiTFSI-G4 electrolyte and corresponding simulated ¹H NMR spectra from DFT-calculated shifts. The left column represents the different solvation structures, identified from MD simulations and further geometry optimized using DFT calculations. The black atoms represent carbon, white atoms represent hydrogen, red atoms are oxygen, purple atoms are lithium, navy atoms are nitrogen, yellow atoms are sulfur, and blue atoms, fluorine. The right column depicts the respective simulated proton spectra, generated based on the DFT-calculated NMR shifts; the spectra are provided for visualization purposes, and scalar (*J*)

coupling effects are not included. The relative peak intensity is chosen analogously to that in Figure 1b to ensure peak positions are visible. The simulation was performed using a single averaged peak value for each proton type within the solvent (Supporting Information 1). The peaks corresponding to each type of proton environment are color coded and labelled.

The DFT-calculated values predict a change in the difference between the chemical shift values of the “A” and “D” resonances as the dominant solvation structure changes from free solvent molecule to two-chain motifs. The chemical shift difference between the “A” and “D” peaks is calculated as 0.283 ppm for a “free” solvent molecule, whereas this increases to 0.324 ppm to 0.362 ppm for the two-chain motif (depending on the specific structure with an average chemical shift difference of 0.343 ppm). The increase is apparently due to the strong coordination of the lithium cation to the oxygen atoms in the central region of the tetraglyme molecule (i.e., within the “A” region) compared to the end region, according to a chelation-like mechanism. This is readily confirmed by inspection of the MD-derived geometries, in which the Li^+ resides closer to the centers of both tetraglyme molecules in order to provide the conformational flexibility for full solvation by six oxygen atoms. Our calculations are consistent with prior experimental and theoretical studies that have reported the tendency of glymes to “wrap around” lithium cations and thereby create a stable, crown-ether like complex cation.¹ We note in passing that minor differences may exist between subtypes of two-chain motifs, i.e., those labelled 1 and 2 in Figure 2. Visually, the difference between the two subtypes of two-chain motif reflects subtle conformational changes, which has been observed in past literature comparing gauche/trans conformers of glymes and glyme–cation complexes.³⁵ The difference between these two double-chain motifs may be identified, however, through calculated differences in the “C” and “D” chemical shift values, but these are too small to be quantified by experimental measurements. Moreover, these solvation structures may undergo conformation interconversion between motif subtypes on a timescale that is short relative to the NMR measurement (i.e., sub-millisecond), based on MD results discussed later.¹⁶ Therefore, we predict that experimental NMR spectra are incapable of distinguishing the two different two-chain motifs, and thus we report the average calculated chemical shift values of these structures.

On the other hand, the predicted spectral difference between free solvent molecules and the one-chain motif is more striking, where in the one-chain motif the “A” and “D” chemical shift difference decreases to 0.128 ppm. This significant decrease appears due to the strong coordination of the Li^+ cation to every oxygen of the tetraglyme molecule, exhibiting a cyclo-like behavior, and thus a much more uniform proton environment. One unique observation for the single-chain motif is that this is the only structure in which the “A” region does not contain the highest predicted value of the chemical shift; the near-end methylene (CH_2) groups (“B”) are predicted to possess a slightly larger chemical shift. However, the swap between the relative position of the “A” and “B” resonances is small so as not to be experimentally quantifiable via experimental ^1H NMR.

To complement computational-based prediction of the importance of the “A” and “D” chemical shift difference, we performed experimental ^1H NMR measurements of LiTFSI-G4 electrolytes as a function of concentration, paying particular attention to changes in the relative shift difference of the resonances. Figure S1 shows experimental ^1H spectral data acquired with varying lithium cation concentration. As expected, an increasing difference between the “A” and “D” peaks is observed as the concentration increases (as shown in Figure 3a), aligning with the

computational study predicting increasing ^1H shift differences with increasing two-chain motifs. Moreover, experimental spectra show additional J-coupling fine structure within the “A” peak as the concentration increases, affirming the diversification of the experimental solvation structures, with different ^1H NMR chemical shift values, as well as the emergence of two-chain motif #2 (Figure 2), possessing the largest separation between the “C” and “D” chemical shift values.

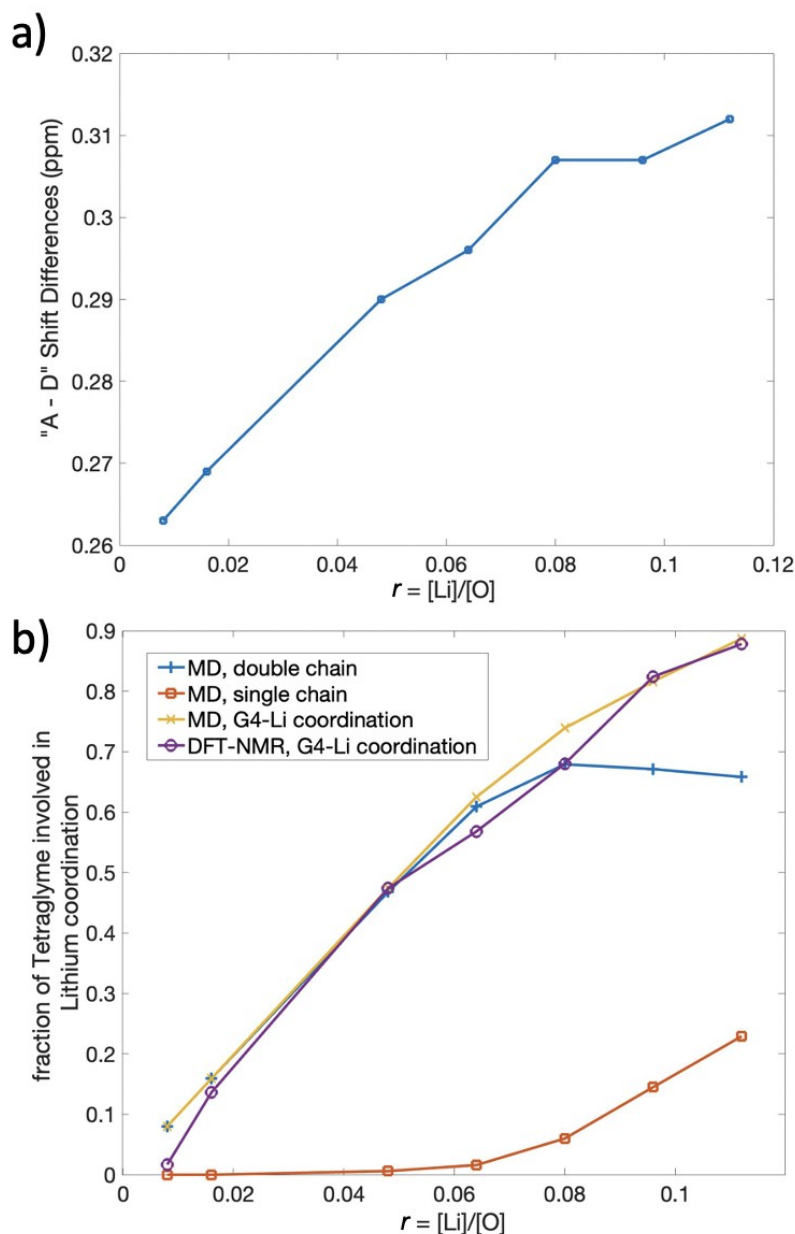


Figure 3. Prediction of fraction of coordinated tetraglyme using MD simulations, ^1H NMR experiments, and DFT calculations. a) Experimental ^1H chemical shift difference between the “A” and “D” resonances of tetraglyme, derived from the ^1H NMR spectra in Figure S1, as a function of the salt concentration, r . b) Comparison of fraction of coordinated tetraglyme as a function of salt concentration, predicted separately from MD simulations directly, and indirectly from the ^1H NMR experiments, using DFT-calculated shifts. The MD-simulated data (blue,

orange, and yellow traces) reflect the fraction of tetraglyme coordinated in two-chain motifs, one-chain motifs, and the sum of these two fractions. The experimental NMR data (purple trace) reflects conversion of the shift differences shown in a) to fraction of coordinating tetraglyme, using ^1H shift values calculated by DFT (see Eq. (1)). The agreement between the total fraction of coordinated tetraglyme (yellow) and the expected values derived from NMR shifts (purple) corroborates the solvation structures and solvation mechanisms of the LiTFSI-G4 system as predicted by MD.

We used the quantitative experimental difference between “A” and “D” chemical shift values to predict the percentage of the free and coordinated solvation structures in the system using the DFT-calculated shift values. Here we used a simple model equation,

$$\Delta\delta = 0.26x + 0.32(1-x) \quad \text{Eq. (1)}$$

where $\Delta\delta$ is the experimental shift difference between the “A” and “D” peak, and x is the fraction of tetraglyme molecules within the free solvent molecule structure, i.e., not undergoing coordination to a lithium cation. Consequently, $(1-x)$ is the fraction of tetraglyme in a two-chain motif structure, where Eq. (1) is valid for the low-concentration regime. Thus, the presence of the single-chain motif is considered insignificant and is omitted from this simple model. We derive the constant 0.26 ppm from subtracting 0.02 from the DFT-calculated “A” - “D” chemical shift difference for free solvent molecules; analogously, the constant 0.32 ppm is derived from subtracting 0.02 from the DFT-calculated “A”- “D” chemical shift difference for two-chain motifs (averaging the two subtypes). The subtraction of 0.02 ppm accounts for the observed difference in our experimental NMR value of neat tetraglyme and the DFT prediction; this may reflect additional effects such as magnetic susceptibility or temperature-dependent chemical shifts, which were not accounted for in the DFT calculations, or the choice of a limited basis set or functional for reasons of computational time. We argue that this adjustment does not invalidate the use of DFT-calculated shifts, since the DFT calculation is equivalent to the chemical shift difference provided in the NMR spectra database (Figure 1b) which indicates that the 0.02 ppm difference is due to external experimental parameters related to our specific NMR measurements.

Just as the combination of ^1H NMR and DFT provides a predicted fraction of coordinated solvent, the MD simulation results also yields the percentage of tetraglyme solvation motifs as a function of *lithium cation concentration* in the LiTFSI-G4 system. Comparing solvent versus cation solvation affords further tests of the solvation constructs. Figure 3b depicts the comparison between the fraction of tetraglyme within differing solvation motifs as predicted by MD simulations, as well as based on the combination of DFT calculations with experimental NMR data. The calculated fraction of two-chain motifs as predicted by MD simulation (blue trace) increases significantly with salt concentration before levelling off. The fraction of tetraglyme molecules that are coordinated to lithium ions, in both double- and single-chain motifs, increases monotonically (yellow trace). The agreement between these two fractions from the dilute limit to around $r \approx 0.08$ shows that the solvation structure of the lower-concentration region is dominated by two-chain motifs and free solvent molecules. Consequently, the model equation we have used to understand the lower-concentration regions is corroborated, despite the

absence of a term corresponding to the single-chain motif. The absence of single-chain motif in the lower-concentration region is also supported by the MD data (orange trace), showing the fraction of tetraglyme in this motif is negligible when the lithium cation concentration is small and increases gradually as the concentration increases beyond $r = 0.08$. Promisingly, the DFT/NMR-predicted fraction of two-chain motifs (purple trace) follows an identical trend to the MD dataset up until $r = 0.08$. Therefore, we conclude that the MD methodology provides a reliable depiction of the local solvation structure of the LiTFSI-G4 electrolyte system in the low-concentration region ($r < 0.08$). Moreover, we reiterate that the LiTFSI-G4 electrolyte system in the lower-concentration region is dominated by two-chain motifs with a 2:1 ratio between tetraglyme molecule and the lithium ion. The agreement between the DFT-NMR dataset and the total fraction of coordinated tetraglyme is striking; this may indicate that the much longer-lived two-chain motif (as discussed later) remains the dominant lifetime-weighted contribution to the appearance of the NMR spectra, despite a global decrease from MD trajectories.

The simple model herein is suitable in the lower-concentration regime, yet may deviate at higher concentrations. This static model may be insufficient to predict the fraction of coordinated tetraglyme at higher concentrations using the DFT/NMR methodology owing to the increase of the single-chain motifs with increasing concentration. However, this explanation cannot account entirely for the discrepancy, as based on the DFT-calculated shifts (Figure 2), the average chemical shift difference should decrease with increasing fraction of tetraglyme within one-chain motifs, in contrast to the experimental data (Figure 3a). Possibilities for the deviation include the tendency of the MD simulation to overestimate the one-chain motif fraction, or the need to account for residence times of the different motifs as discussed below. Future models should consider chemical shift differences weighted by expected lifetimes of the motifs.

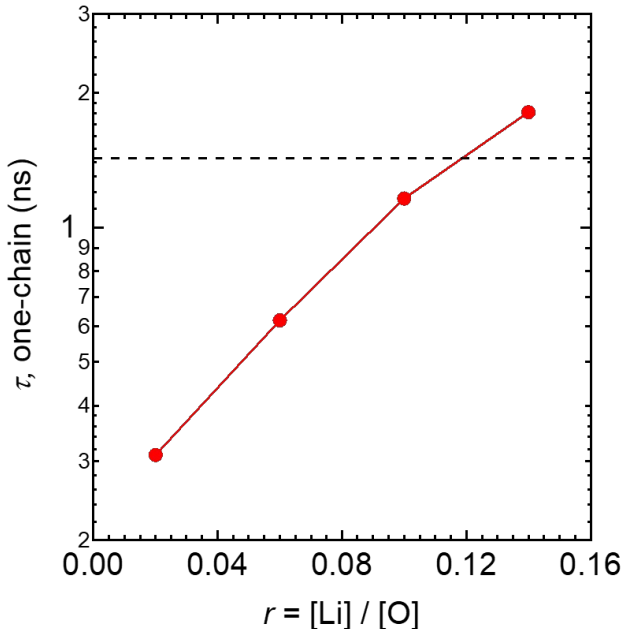


Figure 4. MD-simulated lifetimes of one-chain (ion pair) solvation motifs in LiTFSI-G4 as a function of salt concentration, r ; the one-chain motif residence time τ is extracted by fitting the stretched exponential function $C_{pair}(t) = \exp(-t/\tau)^\beta$ to autocorrelation functions obtained from

the MD simulations (Figure S2b).³¹ The dashed line indicates the inverse of the Larmor frequency used in the NMR experiments; the intersection with the MD data (red trace) indicates the salt concentration at which a maximum in the ¹H spin-lattice relaxation rate would be expected (c.f. Figure S3).

Finally, we probed the dynamics of the solvation structures in the LiTFSI-G4 system through analysis of residence times in the MD simulations, in combination with experimental NMR relaxometry measurements. For both the two-chain and one-chain motifs, autocorrelation functions were calculated, providing a measure of the timescale of G4 molecules that continuously reside within the same motif. As shown in Figure S2a, typical residence times of the two-chain motifs are $\sim 2 \mu\text{s}$ (at $r = 0.02$), decreasing to $\sim 0.2 \mu\text{s}$ (at $r = 0.14$). On the other hand, residence times of the one-chain motif are much shorter (Figure S2b), ranging from 0.31 ns (at $r = 0.02$) up to 1.81 ns (at $r = 0.14$), as depicted in Figure 4. Such values are of the right timescale, i.e., similar to the inverse of the ¹H Larmor frequency in this study (1.4 ns), to provide a contribution to spin-lattice relaxation. Note that while one-chain motif reorganization is not the dominant motional mechanism, and primarily depends upon anion dynamics (rather than the longer-lived cation–solvent complex), the presence of a motional process at the Larmor frequency nonetheless provides a mechanism contributing to ¹H T_1 relaxation of the solvent.³⁶ We speculated that the one-chain motif dynamics predicted by MD could therefore be confirmed by ¹H spin-lattice relaxation measurements.

Figure S3 depicts the ¹H spin-lattice relaxation rates in tetraglyme for the three ¹H resonances that could be easily resolved, corresponding to the "A", "C", and "D" proton environments (Figure 1). In general, an increase in the relaxation rates is observed with increasing salt concentration, suggesting the relaxation behavior is in the fast motion limit, i.e., the relevant correlation times for motion and/or motif reorganization are shorter than $(700 \text{ MHz})^{-1} \approx 1.4 \text{ ns}$. However, a shallow maximum in the R_1 relaxation time is observed at $r \approx 0.12$ for the "A" and "C" resonances, implying that at this concentration, the motional correlation time is $\sim 1.4 \text{ ns}$. This value is in excellent agreement with the one-chain motif residence time at comparable concentration (Figure 4), suggesting that the MD simulations indeed capture the relevant dynamics that dominate T_1 relaxation times. The concurrence between MD and experimental NMR measurements provides confidence in the ability of the present simulation model to provide meaningful information about solvation in concentrated electrolyte systems, and will inform future complementary techniques that combine DFT-calculated chemical shifts with dynamic information, going beyond the "static" MD snapshots of tetraglyme fractions considered here.

Conclusion

To connect the computational-based understanding of LiTFSI-G4 electrolytes with experimental NMR measurements, we have performed complementary MD simulations, DFT calculations, and ¹H NMR spectroscopy on this system as a function of Li-ion concentration ($r = [\text{Li}^+]/[\text{O}] < 0.12$, i.e., less than 2.5 *m* or 2 M). Use of MD simulation pinpoints aspects of the solvation structures and dynamics that could be validated by NMR.

In particular, we obtained MD-derived solvation structures of the tetraglyme solvent molecules as a function of lithium cation concentration.¹⁶ DFT-calculated ¹H NMR shifts of these

structures showed that the local tetraglyme environment and the corresponding oxygen coordination to the lithium ion strongly affects the ^1H NMR spectra, specifically the resonances arising from ^1H in the central region of the solvent molecule that most strongly coordinates with Li^+ . Experimentally, a relative change in the shift of this resonance was observed, supporting findings from DFT calculations. As a quantitative validation of the computational simulations and calculations, we compared MD-simulated results to predicted values using NMR and DFT. Using a simple model employing the DFT-calculated shifts, we converted experimental NMR shifts to fraction of cation-coordinated tetraglyme, which could be compared directly to MD-simulation-based fractions. Agreement between the datasets from these complementary approaches was shown for the low concentration region ($r < 0.08$). The MD simulations suggest the coordination behavior of the tetraglyme solvent molecules closely matches the experimental LiTFSI-G4 system, as quantified by the relative change in ^1H NMR shift values. Further corroboration is provided by consideration of the dynamics of the solvation structures, comparing MD-derived residence times with ^1H spin-lattice (T_1) relaxation measurements.

In conclusion, we validate a complementary experimental and computational methodology as a reliable method of understanding solvation mechanisms and dynamics of the LiTFSI-G4 electrolyte system in the moderately-concentrated regime. In this low-concentration electrolyte system, two-chain motifs are the dominant solvation structure and comprise the main influence on the ^1H NMR spectra of tetraglyme. Future work is needed to demonstrate the validity of the methodology in higher concentration regimes, in which more diverse and complicated solvation structures may arise. We further argue that the work opens up the possibility of the use of spectroscopy in extracting information about the probability of certain motifs as well as the corresponding lifetime of each motif.

Acknowledgements

This work was intellectually led by the Joint Center for Energy Storage Research (JCESR), an Energy Innovation Hub funded by the U.S. Department of Energy (DOE), Office of Science, Basic Energy Sciences (BES). We thank Dr. Hasan Celik and UC Berkeley's NMR facility in the College of Chemistry (CoC-NMR) for spectroscopic assistance, with instruments supported by the National Science Foundation under Grant No. 2018784. The DFT calculations in this work were performed at the UC Berkeley Molecular Graphics and Computational Facility (MGCF), funded by NIH S10OD023532. Additional computational hours were provided by the Savio cluster at UC Berkeley, and the Lawrencium cluster at LBNL, which is supported by the Office of Science, Office of Basic Energy Sciences, of the U. S. Department of Energy under Contract No. DE-AC02-05CH11231.

References

- (1) Thum, A.; Heuer, A.; Shimizu, K.; Canongia Lopes, J. N. Solvate Ionic Liquids Based on Lithium Bis(Trifluoromethanesulfonyl)Imide-Glyme Systems: Coordination in MD Simulations with Scaled Charges. *Phys. Chem. Chem. Phys.* **2020**, 22 (2), 525–535. <https://doi.org/10.1039/C9CP04947A>.

- (2) Wasserscheid, P.; Keim, W. Ionic Liquids—New “Solutions” for Transition Metal Catalysis. *Angew. Chem.* **2000**, *39* (21), 3772–3789. [https://doi.org/10.1002/1521-3773\(20001103\)39:21<3772::AID-ANIE3772>3.0.CO;2-5](https://doi.org/10.1002/1521-3773(20001103)39:21<3772::AID-ANIE3772>3.0.CO;2-5).
- (3) Castner, E. W.; Wishart, J. F. Spotlight on Ionic Liquids. *J. Chem. Phys.* **2010**, *132* (12), 120901. <https://doi.org/10.1063/1.3373178>.
- (4) Eftekhari, A.; Liu, Y.; Chen, P. Different Roles of Ionic Liquids in Lithium Batteries. *J. Power Sources* **2016**, *334*, 221–239. <https://doi.org/10.1016/j.jpowsour.2016.10.025>.
- (5) Méndez-Morales, T.; Carrete, J.; Cabeza, Ó.; Russina, O.; Triolo, A.; Gallego, L. J.; Varela, L. M. Solvation of Lithium Salts in Protic Ionic Liquids: A Molecular Dynamics Study. *J. Phys. Chem. B* **2014**, *118* (3), 761–770. <https://doi.org/10.1021/jp410090f>.
- (6) Angell, C. A.; Byrne, N.; Belieres, J.-P. Parallel Developments in Aprotic and Protic Ionic Liquids: Physical Chemistry and Applications. *Acc. Chem. Res.* **2007**, *40* (11), 1228–1236. <https://doi.org/10.1021/ar7001842>.
- (7) Nakamoto, H.; Watanabe, M. Brønsted Acid–Base Ionic Liquids for Fuel Cell Electrolytes. *Chem Commun* **2007**, No. 24, 2539–2541. <https://doi.org/10.1039/B618953A>.
- (8) Frömling, T.; Kunze, M.; Schönhoff, M.; Sundermeyer, J.; Røling, B. Enhanced Lithium Transference Numbers in Ionic Liquid Electrolytes. *J. Phys. Chem. B* **2008**, *112*, 12985–12990.
- (9) Yoshida, K.; Tsuchiya, M.; Tachikawa, N.; Dokko, K.; Watanabe, M. Change from Glyme Solutions to Quasi-Ionic Liquids for Binary Mixtures Consisting of Lithium Bis(Trifluoromethanesulfonyl)Amide and Glymes. *J. Phys. Chem. C* **2011**, *115* (37), 18384–18394. <https://doi.org/10.1021/jp206881t>.
- (10) Mandai, T.; Yoshida, K.; Ueno, K.; Dokko, K.; Watanabe, M. Criteria for Solvate Ionic Liquids. *Phys. Chem. Chem. Phys.* **2014**, *16* (19), 8761. <https://doi.org/10.1039/c4cp00461b>.
- (11) Ueno, K.; Yoshida, K.; Tsuchiya, M.; Tachikawa, N.; Dokko, K.; Watanabe, M. Glyme–Lithium Salt Equimolar Molten Mixtures: Concentrated Solutions or Solvate Ionic Liquids? *J. Phys. Chem. B* **2012**, *116* (36), 11323–11331. <https://doi.org/10.1021/jp307378j>.
- (12) Tamura, T.; Yoshida, K.; Hachida, T.; Tsuchiya, M.; Nakamura, M.; Kazue, Y.; Tachikawa, N.; Dokko, K.; Watanabe, M. Physicochemical Properties of Glyme–Li Salt Complexes as a New Family of Room-Temperature Ionic Liquids. *Chem. Lett.* **2010**, *39* (7), 753–755. <https://doi.org/10.1246/cl.2010.753>.
- (13) Wichmann, L.; Brinkmann, J.; Luo, M.; Yang, Y.; Winter, M.; Schmich, R.; Placke, T.; Gomez-Martin, A. Improved Capacity Retention for a Disordered Rocksalt Cathode via Solvate Ionic Liquid Electrolytes. *Batter. Supercaps* **2022**. <https://doi.org/10.1002/batt.202200075>.
- (14) Hayamizu, K.; Akiba, E.; Bando, T.; Aihara, Y. ¹H, ⁷Li, and ¹⁹F Nuclear Magnetic Resonance and Ionic Conductivity Studies for Liquid Electrolytes Composed of Glymes and Polyetheneglycol Dimethyl Ethers

- of CH₃O(CH₂CH₂O)NCH₃ (N=3–50) Doped with LiN(SO₂CF₃)₂. *J. Chem. Phys.* **2002**, *117* (12), 5929–5939. <https://doi.org/10.1063/1.1501279>.
- (15) Henderson, W. A.; Seo, D. M.; Han, S.-D.; Borodin, O. Electrolyte Solvation and Ionic Association. VII. Correlating Raman Spectroscopic Data with Solvate Species. *J. Electrochem. Soc.* **2020**, *167* (11), 110551. <https://doi.org/10.1149/1945-7111/aba44a>.
- (16) Halat, D. M.; Fang, C.; Hickson, D.; Mistry, A.; Reimer, J. A.; Balsara, N. P.; Wang, R. Electric-Field-Induced Spatially Dynamic Heterogeneity of Solvent Motion and Cation Transference in Electrolytes. *Phys. Rev. Lett.* **2022**, *128* (19), 198002. <https://doi.org/10.1103/PhysRevLett.128.198002>.
- (17) Frisch, M. J. et al. Gaussian 16, Revision C.01, Gaussian, Inc., Wallingford CT, (2019).
- (18) Hanwell, M. D.; Curtis, D. E.; Lonie, D. C.; Vandermeersch, T.; Zurek, E.; Hutchison, G. R. Avogadro: An Advanced Semantic Chemical Editor, Visualization, and Analysis Platform. *J. Cheminformatics* **2012**, *4* (1), 17. <https://doi.org/10.1186/1758-2946-4-17>.
- (19) Halgren, T. A. Merck Molecular Force Field. I. Basis, Form, Scope, Parameterization, and Performance of MMFF94. *J. Comput. Chem.* **1996**, *17* (5–6), 490–519. [https://doi.org/10.1002/\(SICI\)1096-987X\(199604\)17:5/6<490::AID-JCC1>3.0.CO;2-P](https://doi.org/10.1002/(SICI)1096-987X(199604)17:5/6<490::AID-JCC1>3.0.CO;2-P).
- (20) Rappe, A. K.; Casewit, C. J.; Colwell, K. S.; Goddard, W. A.; Skiff, W. M. UFF, a Full Periodic Table Force Field for Molecular Mechanics and Molecular Dynamics Simulations. *J. Am. Chem. Soc.* **1992**, *114* (25), 10024–10035. <https://doi.org/10.1021/ja00051a040>.
- (21) Becke, A. D. Density-Functional Exchange-Energy Approximation with Correct Asymptotic Behavior. *Phys. Rev. A* **1988**, *38* (6), 3098–3100. <https://doi.org/10.1103/PhysRevA.38.3098>.
- (22) Lee, C.; Yang, W.; Parr, R. G. Development of the Colle-Salvetti Correlation-Energy Formula into a Functional of the Electron Density. *Phys. Rev. B* **1988**, *37* (2), 785–789. <https://doi.org/10.1103/PhysRevB.37.785>.
- (23) Wu, H.; Wick, C. D. Computational Investigation on the Role of Plasticizers on Ion Conductivity in Poly(Ethylene Oxide) LiTFSI Electrolytes. *Macromolecules* **2010**, *43* (7), 3502–3510. <https://doi.org/10.1021/ma902758w>.
- (24) Wick, C. D.; Theodorou, D. N. Connectivity-Altering Monte Carlo Simulations of the End Group Effects on Volumetric Properties for Poly(Ethylene Oxide). *Macromolecules* **2004**, *37* (18), 7026–7033. <https://doi.org/10.1021/ma049193r>.
- (25) Canongia Lopes, J. N.; Pádua, A. A. H.; Shimizu, K. Molecular Force Field for Ionic Liquids IV: Trialkylimidazolium and Alkoxycarbonyl-Imidazolium Cations; Alkylsulfonate and Alkylsulfate Anions. *J. Phys. Chem. B* **2008**, *112* (16), 5039–5046. <https://doi.org/10.1021/jp800281e>.
- (26) Abraham, M. J.; Murtola, T.; Schulz, R.; Páll, S.; Smith, J. C.; Hess, B.; Lindahl, E. GROMACS: High Performance Molecular Simulations through

- Multi-Level Parallelism from Laptops to Supercomputers. *SoftwareX* **2015**, 1–2, 19–25. <https://doi.org/10.1016/j.softx.2015.06.001>.
- (27) Bussi, G.; Donadio, D.; Parrinello, M. Canonical Sampling through Velocity Rescaling. *J. Chem. Phys.* **2007**, 126 (1), 014101. <https://doi.org/10.1063/1.2408420>.
- (28) Berendsen, H. J. C.; Postma, J. P. M.; van Gunsteren, W. F.; DiNola, A.; Haak, J. R. Molecular Dynamics with Coupling to an External Bath. *J. Chem. Phys.* **1984**, 81 (8), 3684–3690. <https://doi.org/10.1063/1.448118>.
- (29) Hess, B.; Bekker, H.; Berendsen, H. J. C.; Fraaije, J. G. E. M. LINCS: A Linear Constraint Solver for Molecular Simulations. *J. Comput. Chem.* **1997**, 18 (12), 1463–1472. [https://doi.org/10.1002/\(SICI\)1096-987X\(199709\)18:12<1463::AID-JCC4>3.0.CO;2-H](https://doi.org/10.1002/(SICI)1096-987X(199709)18:12<1463::AID-JCC4>3.0.CO;2-H).
- (30) Darden, T.; York, D.; Pedersen, L. Particle Mesh Ewald: An $N \cdot \log(N)$ Method for Ewald Sums in Large Systems. *J. Chem. Phys.* **1993**, 98 (12), 10089–10092. <https://doi.org/10.1063/1.464397>.
- (31) Borodin, O.; Smith, G. D. Li⁺ Transport Mechanism in Oligo(Ethylene Oxide)s Compared to Carbonates. *J. Solut. Chem.* **2007**, 36 (6), 803–813. <https://doi.org/10.1007/s10953-007-9146-1>.
- (32) SDBSWeb : <https://Sdbs.Db.Aist.Go.Jp> (National Institute of Advanced Industrial Science and Technology, 05.12.2022).
- (33) Günther, H. *NMR Spectroscopy: Basic Principles, Concepts and Applications in Chemistry*; John Wiley & Sons, 2013.
- (34) Ediger, M. D. Spatially Heterogeneous Dynamics in Supercooled Liquids. *Annu. Rev. Phys. Chem.* **2000**, 51 (1), 99–128. <https://doi.org/10.1146/annurev.physchem.51.1.99>.
- (35) Dong, H.; Hyun, J.-K.; Rhodes, C. P.; Frech, R.; Wheeler, R. A. Molecular Dynamics Simulations and Vibrational Spectroscopic Studies of Local Structure in Tetraglyme:Sodium Triflate (CH₃O(CH₂CH₂O)₄CH₃:NaCF₃SO₃) Solutions. *J. Phys. Chem. B* **2002**, 106 (18), 4878–4885. <https://doi.org/10.1021/jp013914w>.
- (36) Hinz, Y.; Böhmer, R. Deuteron Magnetic Resonance Study of Glyceline Deep Eutectic Solvents: Selective Detection of Choline and Glycerol Dynamics. *J. Chem. Phys.* **2022**, 156 (19), 194506. <https://doi.org/10.1063/5.0088290>.

Supporting Information

Understanding the Solvation Structure of Li-ion Battery Electrolytes Using DFT-based Computation and ^1H NMR Spectroscopy

Julia Im,¹ David M. Halat,^{1,2} Chao Fang,^{1,2} Darby T. Hickson,^{1,2} Rui Wang,^{1,2} Nitash P. Balsara,^{1,2} Jeffrey A. Reimer^{1,2,*}

¹*Department of Chemical and Biomolecular Engineering, University of California, Berkeley, Berkeley, California 94720, United States*

²*Materials Sciences Division and Joint Center for Energy Storage Research (JCESR), Lawrence Berkeley National Laboratory, Berkeley, California 94720, United States*

* reimer@berkeley.edu

Supporting Information 1 DFT-based predictions of ¹H NMR chemical shifts

Gaussian software was used to perform NMR calculations for the different solvation motifs. Single tetraglyme molecules were selected to perform the geometry optimization and NMR calculations for neat tetraglyme. Single lithium ion with two tetraglyme molecules were selected to perform the calculation for the two-chain motifs. Last, single TFSI anion, two lithium ions, and two tetraglyme molecules were selected to perform the calculation for the one-chain motif.

Category corresponds to the characterizations of the proton environment with “D” representing the end methyl groups, “A” representing the middle methylene groups, and “B” and “C” representing the methylene groups between “A” and “D”. The proton labelled number represent the auto-generated labels by the Gaussian software when running the NMR calculation.

Table S1. ¹H chemical shifts of the individual protons in neat tetraglyme.

Category	Proton Labelled Number	¹ H Shift (ppm)
D	16	3.9542
D	17	3.5401
D	18	3.5533
C	19	3.7543
C	20	3.817
D	21	3.8711
B	21	4.2007
D	22	3.7415
B	22	3.7651
D	23	4.204
A	23	4.3224
C	24	3.7381
A	24	3.8384
C	25	4.2827
A	25	4.115
B	26	4.4792
A	26	3.7829
B	27	3.9291
A	27	3.9172
A	28	4.2849
A	28	3.9521
A	29	3.9351
A	29	3.9479
A	30	3.8993
A	30	3.9115
A	31	4.233
B	31	3.7481
A	32	3.8869
B	32	4.0667
A	33	4.7403
C	33	4.3138
A	34	4.0766
C	34	3.6658
A	35	3.7805
D	35	3.8766
B	36	4.0446
D	36	3.4308
B	37	4.0367
D	37	3.7876

Table S2. ¹H chemical shifts of individual protons in double chain motif #1.

C	49	3.8013
C	50	3.6363
D	51	4.1319
D	52	3.3885
D	53	3.472
D	54	4.0479
D	55	3.4744
D	56	3.5013
C	57	3.981
C	58	3.8007
B	59	4.1158
B	60	4.2397
A	61	4.1033
A	62	4.3702
A	63	3.8331
A	64	4.5511
A	65	4.7922
A	66	3.5003
A	67	3.7973
A	68	4.7983
B	69	4.6091
B	70	3.81
C	71	3.7157
C	72	4.1128
D	73	4.3492
D	74	3.7537
D	75	3.6524

Table S3. ¹H chemical shifts of individual protons in double chain motif #2

Category	Proton Labelled Number	¹ H Shift (ppm)
D	32	3.7681
D	33	4.2084
D	34	3.8559
C	35	3.7197
C	36	4.3123
B	37	4.4435
B	38	3.9395
A	39	4.305

A	40	3.9253
A	41	3.8884
A	42	4.2431
A	43	3.8814
A	44	4.7318
A	45	4.0572
A	46	4.0567
B	47	3.7896
B	48	3.6448
C	49	4.1354
C	50	3.4147
D	51	3.4222
D	52	3.524
D	53	4.0399
D	54	3.4408
D	55	3.9514
D	56	3.8489
C	57	4.0861
C	58	4.2424
B	59	4.1381
B	60	4.2938
A	61	3.8212
A	62	4.6002
A	63	4.0249
A	64	3.8472
A	65	4.8148
A	66	3.4533
A	67	3.7965
A	68	4.8253
B	69	4.6113
B	70	3.8103
C	71	3.7182
C	72	4.1131
D	73	4.3585
D	74	3.7566
D	75	3.6404

Table S4. ¹H chemical shifts of individual protons in the single chain motif

Category	Proton	¹ H Shift
----------	--------	----------------------

	Labelled Number	(ppm)
D	48	4.6445
D	49	3.7683
D	50	3.7614
C	51	4.2732
C	52	3.6449
B	53	3.7364
B	54	4.697
A	55	3.5373
A	56	4.7619
A	57	4.2751
A	58	3.5823
A	59	3.8743
A	60	4.3549
A	61	4.2474
A	62	3.935
B	63	4.3958
B	64	3.8804
C	65	3.7712
C	66	4.803
D	67	4.2829
D	68	3.8079
D	69	4.2339
D	70	3.6988
D	71	4.6502
D	72	3.8437
C	73	3.6409
C	74	4.1602
B	75	4.8566
B	76	3.7274
A	77	5.593
A	78	3.7124
A	79	3.9269
A	80	3.9411
A	81	4.0032
A	82	4.0895
A	83	5.164
A	84	3.8457
B	85	3.8273

B	86	4.6391
C	87	4.7636
C	88	3.5022
D	89	4.1768
D	90	4.0227
D	91	3.7103

Supporting Information 2 Selection of functional/basis set combination for the DFT calculation

Given the number of calculations and conformations explored in this work, the B3LYP/6-31G(d) functional/basis set combination was optimal for our purpose. To validate the use of the following functional/basis set, we performed DFT calculations using varying functional/basis set on the neat tetraglyme system and compared with the experimental results. Our results show that the usage of B3LYP/6-31G(d) accurately reflects the experimental results and is still time efficient.

Experimental neat tetraglyme NMR spectra based on the NMR spectral database

Proton Classification	Chemical Shift (ppm)
A	3.658
B	3.650
C	3.550
D	3.376

“A-D” Difference in Chemical Shift: 0.282

DFT-based NMR spectra (B3LYP/6-31G(d))

1. Proton Classification	Chemical Shift (ppm)
A	3.973
B	3.945
C	3.888
D	3.690

“A-D” Difference in Chemical Shift: 0.283

Calculation done on varying functional/basis set

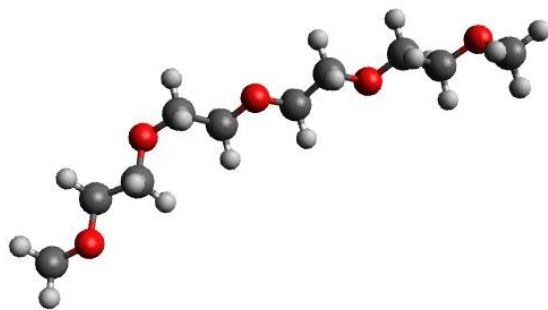
Functional	DFT Basis	Calculated energy (A.U.)	A-D Difference in Chemical Shift (ppm)
B3LYP	6-31G(d)	-770.3440	0.283
B3LYP	6-31G(d,p)	-770.3732	0.252
B3LYP	6-311+G(d,p)	-770.6002	0.224
B3LYP	6-311++G(3df,2p)	-770.6360	0.195
B3LYP	Aug-cc-pVTZ	-770.6567	0.196
RHF	6-31G(d)	---	0.0655
AM1	6-31G(d)	-0.3823*	NMR calculations not implemented in Gaussian
PM3	6-31G(d)	-765.7160	NMR calculations not implemented in Gaussian
MP2	6-31G(d)	-765.7077	0.250
CCSD	(in progress)	---	(in progress)

* Note that for AM1, the energies reported represent heats of formation and cannot be compared directly with the other methods.

Supporting Information 3 Selection of neat tetraglyme conformers

For our study, the following motif was used for the calculations related to neat tetraglyme molecules. This conformer is generated by geometry-optimizing the tetraglyme molecule from the linear position to its energy minimum.

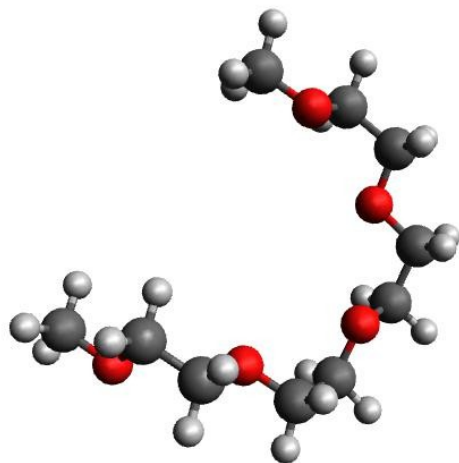
Conformer 1



<T T T T> conformation (all oxygen atoms are anti/trans)

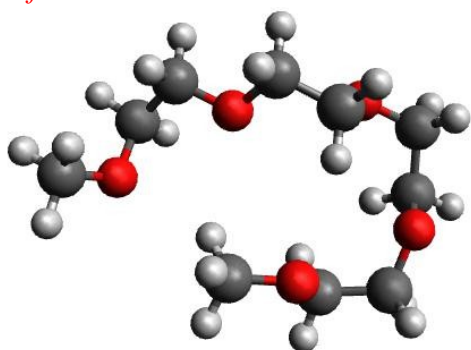
Following are conformers 2-4, which are other possible conformers of neat tetraglyme, as derived by MD simulations. These conformers were chosen from random snapshots from MD simulations in which the tetraglyme molecules were not coordinated to Li^+ , so they represent common conformers of neat G4. Within each of conformers 2-4, all oxygen atoms are arranged in a gauche manner. The conformers differ in that two dihedral angles (positive or negative) are possible for a gauche configuration; we have explored a representative sample of conformers of this type as revealed by the MD simulations.

Conformer 2



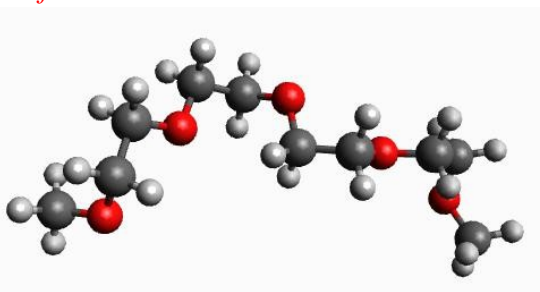
<G G G G> conformation (all oxygen atoms are gauche)

Conformer 3



<G G G G> conformation (all oxygen atoms are gauche)

Conformer 4



<G G G G> conformation (all oxygen atoms are gauche)

The NMR spectra for each neat tetraglyme conformers were performed and compared based on the “A-D” chemical shift difference. The experimental data of comparison as the “A-D” difference is 0.282 ppm. Conformer 1 strongly agrees with the experimental data. Moreover, the average of the various conformers (average of conformer 1-4, average of conformer 2-4) also resembles the experimental data. Therefore, we can validate the use of conformer 1 as a representative conformer for neat tetraglyme.

Conformer	“A-D” Difference in Chemical Shift (ppm)
1	0.283
2	0.160
3	0.346
4	0.332
2-4 average	0.279
1-4 average	0.281

Supporting Information 4 MD Simulation force field parameters

(1) Lennard-Jones parameters and partial charges

Particles	Particle type	Charge (e)	σ_i (nm)	ϵ_i (kJ/mol)
Lithium cation	Li ⁺	1.00	0.140	1.67360e+0
Carbon atom (TFSI)	CT	0.35	0.350	2.76140e-1
Nitrogen atom (TFSI)	N	-0.66	0.325	7.11280e-1
Oxygen atom (TFSI)	O	-0.53	0.296	8.78640e-1
Fluorine atom (TFSI)	F	-0.16	0.295	2.21750e-1
Sulfur atom (TFSI)	S	1.02	0.355	1.04600e+0
CH3 bead (G4)	CET	0.25	0.375	8.15242e-1
Oxygen atom (G4)	OET	0.50	0.285	4.57534e-1
CH2 bead (G4)	CHA	0.25	0.395	3.82664e-1

(2) Bonded parameters

(a) Bond stretching

$$V_b(r_{ij}) = \frac{1}{2} k_{ij}^b (r_{ij} - b_{ij})^2$$

Bond type	b (nm)	k^b (kJ/mol/nm ²)
CET-CET	1.540000e-1	NA (fixed bond)
CET-OET	1.410000e-1	NA (fixed bond)
OET-CHA	1.410000e-1	NA (fixed bond)
CT-S	1.818000e-1	1.970000e+5
CT-F	1.323000e-1	3.697000e+5
S-N	1.570000e-1	3.113000e+5
S-OT	1.442000e-1	5.331000e+5

(b) Angle vibration

$$V_a(\theta_{ijk}) = \frac{1}{2} k_{ijk}^a (\theta_{ijk} - \theta_{ijk}^0)^2$$

Angle type	k^a (kJ/mol/rad ²)	θ^0 (degree)
CET-CET-OET	4.184352e+2	112
CET-OET-CET	5.024550e+2	112
CET-OET-CHA	4.184352e+2	112
CT-S-N	8.160000e+2	100.2

CT-S-OT	8.700000e+2	102.6
S-CT-F	6.940000e+2	111.8
S-N-S	6.710000e+2	125.6
N-S-OT	7.890000e+2	113.6
F-CT-F	7.810000e+2	107.1
OT-S-OT	9.690000e+2	118.5

(c) Ryckaert-Bellemans proper dihedral

$$V_{rb}(\phi_{ijkl}) = \sum_{n=0}^5 C_n \left(\cos(\phi_{ijkl} - 180^\circ) \right)^n$$

Dihedral type	c_0 (kJ/mol)	c_1 (kJ/mol)	c_2 (kJ/mol)	c_3 (kJ/mol)	c_4 (kJ/mol)	c_5 (kJ/mol)
CET-CET-OET-CET	7.9532e+0	7.8966e+0	2.7244e+0	-1.8574e+1	0	0
CET-CET-OET-CHA	7.9532e+0	7.8966e+0	2.7244e+0	-1.8574e+1	0	0
OET-CET-CET-OET	3.9514e+0	3.9514e+0	7.9029e+0	0	0	0
CT-S-N-S	4.3690e+0	-2.1179e+1	1.0420e+1	6.3900e+1	0	0
S-N-S-OT	-7.5000e-3	-2.2500e-2	0	3.0000e-2	0	0
F-CT-S-N	6.6100e-1	1.9830e+0	0	-2.6440e+0	0	0
F-CT-S-OT	7.2550e-1	2.1765e+0	0	-2.9020e+0	0	0

Supporting Information 5 Additional NMR and MD results

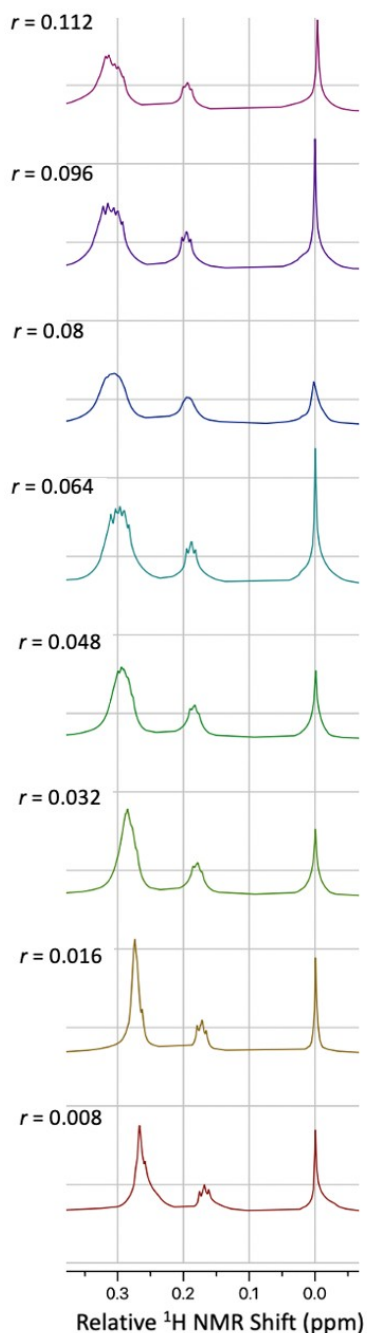


Figure S1. Experimental ^1H NMR spectra of the LiTFSI-G4 system as a function of concentration $r = [\text{Li}^+]/[\text{O}]$; the shift scale is referenced to the lowest-frequency resonance to highlight the concentration-dependent separation between the resonances. That is, the chain-end “D” resonance (right peak) is referenced to 0 ppm to visualize the overall increasing difference between the “A” (middle CH_2 proton) and “D” (chain-end CH_3 proton) peaks as a function of salt concentration, r . The middle peak corresponds to the “C” (near-end CH_2 protons) resonance in Figure 1, which possesses a much weaker dependence of its chemical shift on the salt

concentration. (Note: the position of the “B” resonance overlaps with the more intense signal from “A”.)

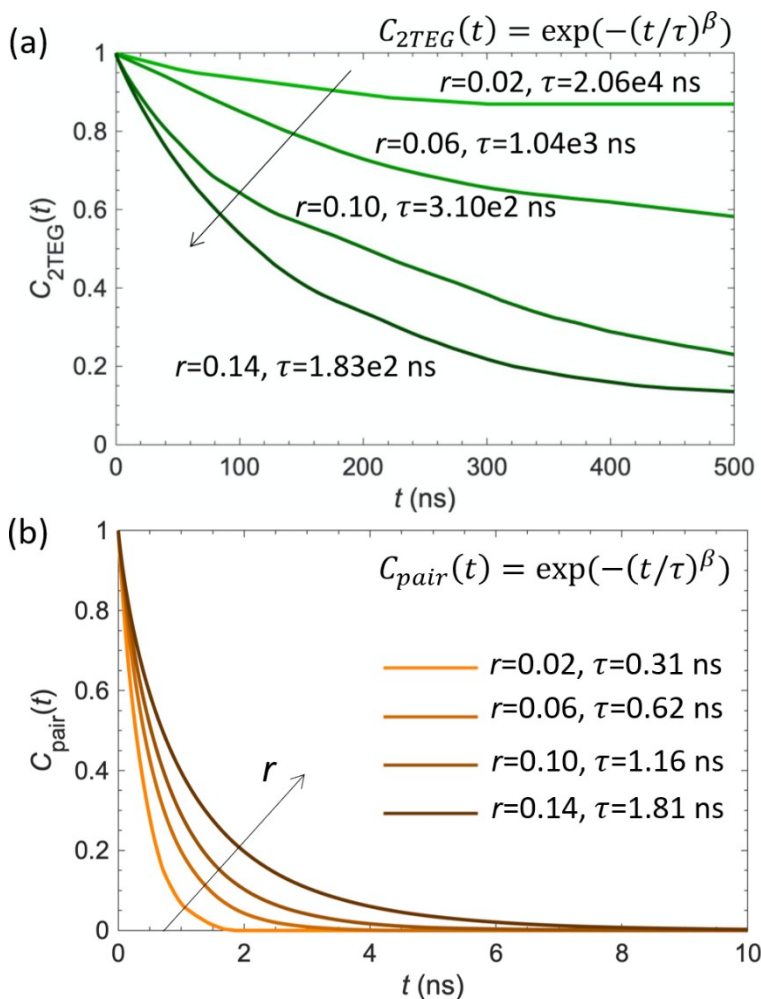


Figure S2. MD-simulated autocorrelation functions for two-chain and one-chain solvation motifs in LiTFSI-G4 as a function of salt concentration r ; (a) the two-chain motif residence times τ are extracted by fitting the exponential function $C_{2TEG}(t) = \exp(-(t/\tau)^\beta)$, and (b) the one-chain motif residence times τ are extracted by fitting the exponential function $C_{pair}(t) = \exp(-(t/\tau)^\beta)$.

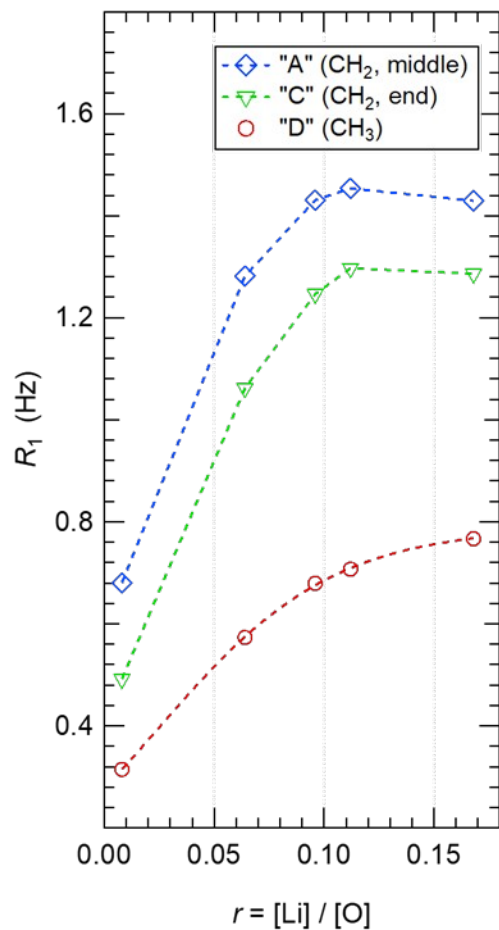


Figure S3. Experimental ^1H R_1 spin-lattice relaxation rates for the “A”, “B”, and “D” ^1H resonances of tetraglyme as a function of salt concentration, r ; a maximum is observed for the former two ^1H environments at $r \approx 0.12$.

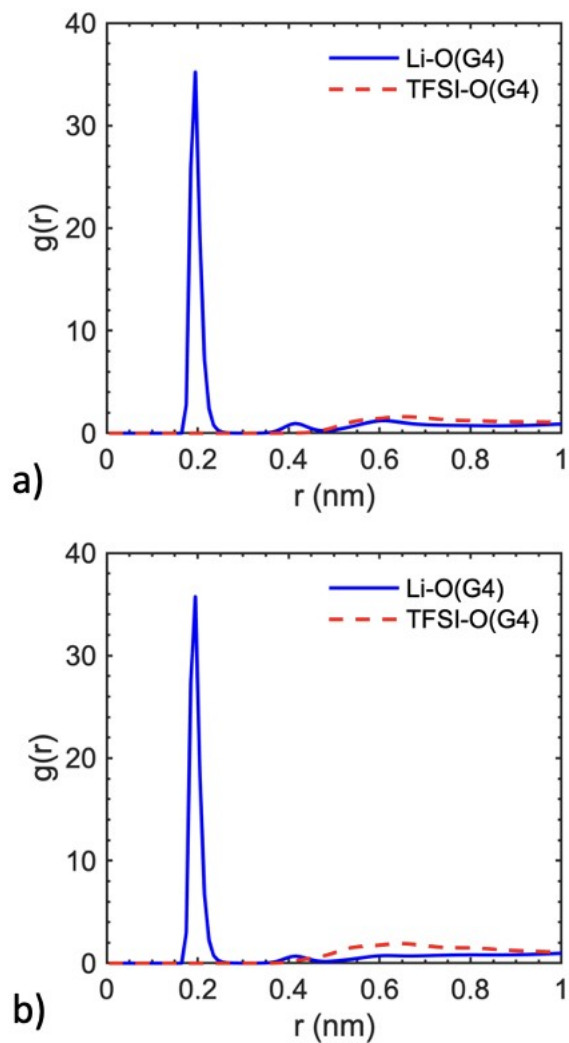


Figure S4. Radial distribution function from MD simulations for LiTFSI-G4 electrolyte system in selected concentrations: (a) $r = 0.048$, and (b) $r = 0.096$. Only long-range interactions between the TFSI⁻ anion and tetraglyme are observed; for tetraglyme molecules, the dominant solvation interaction arises from coordination with Li⁺.

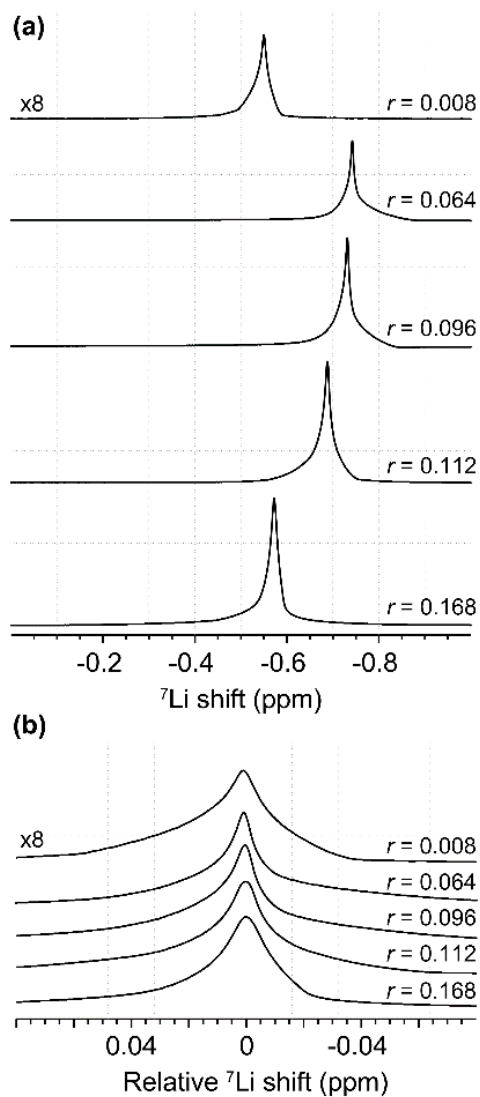


Figure S5. (a) ^7Li NMR spectra of selected LiTFSI/tetraglyme electrolytes as a function of concentration. (b) ^7Li NMR spectra aligned to peak maximum to compare changes in linewidth. Spectra were acquired at 16.4 T.